COBEM 2023 27TH INTERNATIONAL CONGRESS OF MECHANICAL ENGENEERING

ABCM Brazilian Society of Mechanical Sciences and Engineering
27th ABCM International Congress of Mechanical Engineering
December 04-08, 2023, Florianópolis-SC, Brazil

COB-2023-0326
CONSTRUCTAL DESIGN OF AN ISOTHERMAL BODY AND A LID-DRIVEN CAVITY FILLED WITH A METALLIC NANOFLUID

Rafael da Silveira Borahel[1]
Priscila Martta Rodrigues[2]
Flávia Schwarz Franceschini Zinani[3]
Mechanical Engineering Graduate Program, Universidade do Vale do Rio dos Sinos, 93022-750, São Leopoldo, RS, Brazil
rborahel@edu.unisinos.br[1]; priscilamartta@edu.unisinos.br[2]; fzinani@unisinos.br[3]

Luiz Alberto Oliveira Rocha
Mechanical Engineering Graduate Program, Universidade Federal do Rio Grande do Sul, 90040-001, Porto Alegre, RS, Brazil
Computational Modeling Graduate Program, Universidade Federal do Rio Grande, 96203-900, Rio Grande, RS, Brazil
luizrocha@mecanica.ufrgs.br

Abstract. *The present work aims to numerically evaluate and maximize, through the Construtal Design method and the exhaustive search, the convective heat transfer between an isothermal block (IB) and the surrounding flow in a lid-driven cavity. As working fluid, a metallic nanofluid (water + Al2O3) – with different concentrations of Al2O3 particles (ψ = 0, 1, 2 and 3%) – is used. The degrees of freedom admitted for the system are the IB and cavity aspect ratios, while their areas are the constraints. Altogether, 36 different configurations were tested for the problem, resulting in an equal number of numerical simulations solved in the commercial software ANSYS Fluent 2022 R2. Based on the obtained results, it was observed that the convective heat transfer was intensified when the cavity assumed a horizontally elongated shape, with the isothermal block having a tall configuration. Regarding the effects of nanoparticle concentration, it was observed that a higher concentration contributes to improve the convective heat transfer within the cavity. This can be attributed to the modifications that arise in flow properties, particularly in the thermal conductivity, by the addition of nanoparticles to the base fluid.*

Keywords: *constructal design, lid-driven cavity, mixed convection, laminar flow, metallic nanofluid.*

1. INTRODUCTION

Studies related to convective heat transfer in cavities with heated obstacles have been growing, as it is an important research in computational fluid dynamics, being necessary for the development of increasingly complex problems. There are several applications related to convective heat transfer and cavities such as cooling of electronic devices (Kareem and Gao, 2018), solar collectors (Gangawane et al., 2018), nuclear reactors (Kumar et al., 2021) and cooling/ventilation of building environments (Razera et al., 2018). These studies are relevant since they allow to evaluate designs and optimize systems involving thermal exchange in more complex cavities, contributing to scientific and technological advancement. Several studies have sought to understand the interaction between flow and convective heat transfer inside cavities with heated obstacles of different shapes, among them, circular (Rais et al, 2023), elliptical (Younis et al., 2023), square/rectangular (Herouz et al., 2023) and triangular (Alsabery et al., 2020).

The use of Constructal Design for this type of problem aims to analyze which geometry presents the best performance, since Constructal Design is a method of geometric evaluation that is based on the application of constraints and objectives in geometries of finite-dimensional flow systems. The use of this method is intended to deterministically explain that designs found in nature are not random (Bejan and Lorente, 2008). Constructal Design is a method grounded in the physical principle known as the Constructal Law. This law states that for a finite flow system, whether animate or inanimate, to persist over time and survive, its design must evolve in a way that facilitates access for the currents flowing through that system. (Bejan and Lorente, 2008). Razera et al. (2022) numerically investigated heated semi-elliptic blocks within convective channels, employing the Constructal Design. Borahel et al. (2022b) applying Constructal Design analyzed the performance of a rectangular isothermal block inside an adiabatic cavity subjected to mixed convection heat transfer and with unsteady stratification.

In this context, the present work aims to analyze which geometry leads to the best performance a lid-driven cavity subjected to mixed convection, two-dimensional, laminar, incompressible, steady-state Newtonian nanofluid flow. The performance indicator is the dimensionless heat transfer rate (q^*). The geometry investigated is an isothermal block inserted in a lid-driven cavity, subjected to a nanofluid with different concentrations of Al_2O_3 particles, which is varied by applying the Constructive Design method associated with exhaustive search, to obtain which geometry leads to the

best performance. For all simulations $Re = 10^3$, $Gr = 10^5$ and $Ri = 0.1$ were considered. The effect of the cavity ratios ($AR = H/L$), as well as, the isothermal block ratios ($AR_0 = H_0/L_0$) are investigated.

2. METHODOLOGY

2.1 Constructal Design Method

In the present work, the constructal design method (CDM) was used to study the geometry of the proposed problem. In engineering problems, the application of this method occurs through a sequence of steps, resulting in a flowchart (Cunegatto et al., 2023), which is shown in Figure 1. All the steps that integrate the CDM are detailed below, considering the particularities of the studied problem.

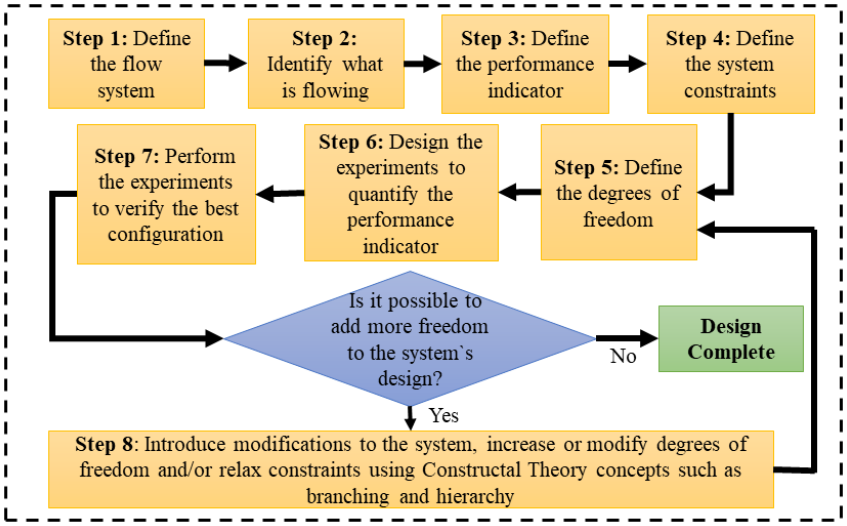

Figure 1. Flowchart of the application of the constructal design method.

Step 1: Define the Flow System

The flow system consists of a lid-driven cavity with an isothermal block (IB) inside. As working fluid, a metallic nanofluid (water + Al_2O_3) – with different concentrations of Al_2O_3 particles (ψ = 0, 1, 2 and 3%) – was used. Figure 2 shows the schematic representation of the two-dimensional computational domain adopted, while Table 1 shows the physical properties of the base fluid (water) and the Al_2O_3 particles.

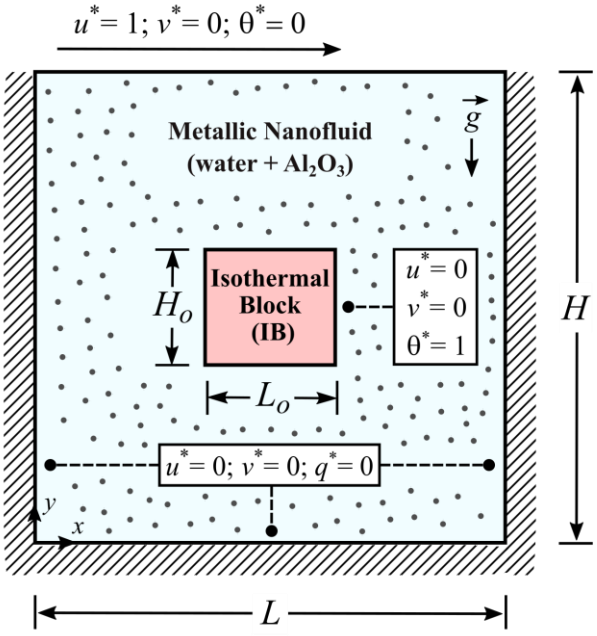

Figure 2. Schematic representation of the computational domain.

Table 1. Physical properties of the base fluid (water) and the Al_2O_3 particles.

Physical Properties	**Water** (1)	**Al_2O_3** (2)
Density (ρ)	998.2 ($kg.m^{-1}$)	3970 ($kg.m^{-1}$)
Dynamic Viscosity (μ)	0.001003 ($kg.m^{-1}.s^{-1}$)	x---x---x---x
Specific Heat (c_p)	4182 ($J.kg^{-1}.K^{-1}$)	765 ($J.kg^{-1}.K^{-1}$)
Thermal Conductivity (k)	0.6 ($W.m^{-1}.K^{-1}$)	40 ($W.m^{-1}.K^{-1}$)
Thermal Expansion Coefficient (β)	0.000207 (K^{-1})	0.00000846 (K^{-1})

(1) Default values of ANSYS Fluent 2022 R2;
(2) Values obtained in Shulepova et al. (2020)

In the system shown in Fig. 2, two mechanisms drive simultaneously the heat transfer between the IB and the nanofluid: forced convection (related to the flow generated by the shear forces resulting from the lid movement) and natural convection (associated with the flow generated by the buoyancy forces that are originated by the temperature gradients of the nanofluid). If these mechanisms have the same relevance, the heat transfer takes place by mixed convection (Prasad and Koseff, 1996; Rodrigues et al., 2020). According to Prasad and Koseff (1996), the Richardson number (*Ri*), given by Gr/Re^2, where *Gr* is the Grashof number (Equation 1) and *Re* is the Reynolds number (Equation 2), is traditionally used to indicate the relative strengths of the forced and natural convection mechanisms in a mixed convection environment. To obtain $Ri = 0.1$, which represents the predominance of the forced mechanism, we assumed *Gr* equals 10^5 and *Re* equals 10^3.

$$Gr = \frac{\vec{g}\Delta T\beta_{nf}(A)^3}{(\nu_{nf})^2} \tag{1}$$

$$Re = \frac{U_{lid}\sqrt{A}}{\nu_{nf}} \tag{2}$$

where $\vec{g}$ is the gravity acceleration, *A* is the cavity area, β_{nf} and ν_{nf} are, respectively, the thermal expansion coefficient and kinematic viscosity of the nanofluid and ΔT is the difference between the temperatures of the IB (T_{IB}) and the lid-driven surface (T_{lid}).

Step 2: Identify the Flow and System's Purpose

As lid-driven cavities – with heated obstacles inside – ideally portray the problem of cooling electronic devices in confined spaces, the purpose of the flow system (Fig. 2) is to promote the heat transfer between the IB and the surrounding flow. Thus, by the constructal theory, the system's design must evolve to facilitate the flow of what keeps it "alive", the convective heat between the IB and the nanofluid.

Step 3: Define the Performance Indicator

For the analysis and quantification of the convective heat transfer inside the cavity, the dimensionless heat transfer rate ($q^* = q/W.\Delta T.k_{nf}$) between the IB and the nanofluid flow was assumed as the performance indicator, where q is the heat transfer rate at the IB walls, *W* is the unitary cavity depth and k_{nf} is the thermal conductivity of the nanofluid.

Step 4: Define the System Constraints

The constraints of the system, which limit its evolution, are the areas of the cavity ($A = H.L$) and the IB ($A_0 = H_0.L_0$). In their dimensionless form, *A* is represented by $H^*.L^* = 1$ and A_0 by the area fraction ($\phi = A_0/A$), which is equal to 1/4. For the sake of clarity, *H* and *L* are the cavity height and length, H_0 and L_0 are the IB height and length, while H^* and L^* are the dimensionless cavity height and length.

Step 5: Define the System Degrees of Freedom (DOF)

To analyze the impact of the system design on the nanofluid flow and the convective heat transfer, enabling its evolution towards a configuration that maximizes q^*, the cavity ($AR = H/L$) and IB ($AR_0 = H_0/L_0$) aspect ratios were adopted as the system degrees of freedom (DOF).

Step 6: Design the Experiments/Simulations to Quantify the System Performance Indicator

The experiments/simulations to evaluate the system performance indicator (q^*) response to the nanoparticles concentration and the system architecture were designed considering four different values for φ (0, 1, 2 and 3%) and three values for AR and AR_0: 0.5 (horizontal shape), 1.0 (square shape) and 1.5 (vertical shape). Altogether, 36 different configurations were tested for the problem, resulting in an equal number of experiments/simulations to be performed.

Step 7: Perform the Experiments/Simulations to Find the Best Problem Configuration

The experiments to find the best problem configuration were carried out computationally, through numerical simulations based on the finite volume method (FVM). To solve the numerical simulations, the commercial software ANSYS Fluent 2022 R2 was used.

Step 8: System's Evolution

Introducing modifications to the system, increasing DOF or relaxing constraints are actions that give greater freedom to the system, allowing its evolution. However, in the present work, the freedom given to the flow system was limited to the DOF analyzed (AR and AR_0), so that the application of the CDM was considered complete after the step 7.

2.2 **Mathematical Model**

The mathematical model implemented to solve the proposed problem is based on the conservative equations of mass, momentum (in x and y directions) and energy, respectively described by Eqs. (3-6) (Shulepova et al., 2020). The nanofluid flow was considered Newtonian, two-dimensional, laminar, incompressible and steady-state. All its physical properties were assumed constant with respect to temperature, apart from density (ρ_{nf}), which was treated as a function temperature – by the Boussinesq approximation – in the buoyance term of the momentum equation in y direction (Eq. 5).

$$\frac{\partial u}{\partial x}+\frac{\partial v}{\partial y}=0 \tag{3}$$

$$\rho_{nf}\left(u\frac{\partial u}{\partial x}+v\frac{\partial u}{\partial y}\right)=-\frac{\partial p}{\partial x}+\mu_{nf}\left(\frac{\partial^2 u}{\partial x^2}+\frac{\partial^2 u}{\partial y^2}\right) \tag{4}$$

$$\rho_{nf}\left(u\frac{\partial v}{\partial x}+v\frac{\partial v}{\partial y}\right)=-\frac{\partial p}{\partial y}+\mu_{nf}\left(\frac{\partial^2 v}{\partial x^2}+\frac{\partial^2 v}{\partial y^2}\right)+\vec{g}(\rho\beta)_{nf}(T-T_{lid}) \tag{5}$$

$$\left(\rho c_p\right)_{nf}\left(u\frac{\partial T}{\partial x}+v\frac{\partial T}{\partial y}\right)=k_{nf}\left(\frac{\partial^2 T}{\partial x^2}+\frac{\partial^2 T}{\partial y^2}\right) \tag{6}$$

where x and y are the Cartesian coordinates in the horizontal and vertical directions, u and v are the nanofluid flow velocities in the horizontal and vertical directions, p is the pressure, T is the temperature, μ_{nf} and $(c_p)_{nf}$ are, respectively, the nanofluid dynamic viscosity and specific heat.

As the physical properties of the nanofluid are dependent on the particle's concentration, the relations presented by Shulepova et al. (2020) were used to calculate the effective properties of the flow. Thus, ρ_{nf} was obtained through Eq. (7), β_{nf} by Eq. (8), $(c_p)_{nf}$ by Eq. (9), k_{nf} by Eq. (10) and μ_{nf} by Eq. (11):

$$\rho_{nf}=(1-\psi)\rho_f+\psi\rho_p \tag{7}$$

$$(\rho\beta)_{nf}=(1-\psi)(\rho\beta)_f+\psi(\rho\beta)_p \tag{8}$$

$$\left(\rho c_p\right)_{nf}=(1-\psi)\left(\rho c_p\right)_f+\psi\left(\rho c_p\right)_p \tag{9}$$

$$k_{nf}=k_f(1+2.944\psi+19.672\psi^2) \tag{10}$$

$$\mu_{nf}=\mu_f(1+4.93\psi+222.4\psi^2) \tag{11}$$

where the subscript f denotes the fluid (water) properties and p the particles (Al_2O_3) properties.

To generalize the problem and its results, the dimensionless forms of the geometric (*x*, *y*, *H*, *L*, H_0 and L_0) and flow parameters (*u* and *v*), temperature (*T*) and pressure (*p*) were obtained, respectively, using the Eqs. (12-15):

$$x^*, y^*, H^*, L^*, H_0^*, L_0^* = \frac{x, y, H, L, H_0, L_0}{\sqrt{A}} \tag{12}$$

$$u^*, v^* = \frac{u, v}{U_{lid}} \tag{13}$$

$$\theta^* = \frac{T - T_{lid}}{T_{IB} - T_{lid}} \tag{14}$$

$$p^* = \frac{p}{\rho_{nf}(U_{lid})^2} \tag{15}$$

where x^* and y^* are the dimensionless Cartesian coordinates in the horizontal and vertical directions, u^* and v^* are the dimensionless flow velocities in the horizontal and vertical directions, θ^* is the dimensionless temperature and p^* is the dimensionless pressure.

Applying the Eqs. (12-15) and assuming the definitions of Prandtl [$Pr_{nf} = (c_p\mu/k)_{nf}$], Re (Eq. 2) and Ri ($Gr/Re^2$) numbers, the conservative equations (Eqs. 3-6) could be rewritten and solved in their dimensionless forms as follows:

$$\frac{\partial u^*}{\partial x^*} + \frac{\partial v^*}{\partial y^*} = 0 \tag{16}$$

$$u^*\frac{\partial u^*}{\partial x^*} + v^*\frac{\partial u^*}{\partial y^*} = -\frac{\partial p^*}{\partial x^*} + \frac{1}{Re}\left(\frac{\partial^2 u^*}{\partial (x^*)^2} + \frac{\partial^2 u^*}{\partial (y^*)^2}\right) \tag{17}$$

$$u^*\frac{\partial v^*}{\partial x^*} + v^*\frac{\partial v^*}{\partial y^*} = -\frac{\partial p^*}{\partial y^*} + \frac{1}{Re}\left(\frac{\partial^2 v^*}{\partial (x^*)^2} + \frac{\partial^2 v^*}{\partial (y^*)^2}\right) + Ri.\theta^* \tag{18}$$

$$u^*\frac{\partial \theta^*}{\partial x^*} + v^*\frac{\partial \theta^*}{\partial y^*} = \frac{1}{RePr}\left(\frac{\partial^2 \theta^*}{\partial (x^*)^2} + \frac{\partial^2 \theta^*}{\partial (y^*)^2}\right) \tag{19}$$

2.2.1 Boundary Conditions

The non-slip condition ($u^* = v^* = 0$) was enforced on all stationary walls of the system, while a constant velocity in the rightward direction ($u^* = 1$) was specified on the lid wall. The adiabatic condition ($q^* = 0$) was applied to the bottom, left, and right walls of the cavity, the lowest temperature ($\theta^* = 0$) was assigned to the lid-driven surface and the highest temperature ($\theta^* = 1$) was set on the IB walls. These boundary conditions are visually depicted in Fig. 2, providing a better understanding of where they were applied.

2.3 **Numerical Model**

As already mentioned, the problem proposed was solved computationally through numerical simulations based on the FVM. All numerical simulations were carried out in the commercial software ANSYS Fluent 2022 R2, where different algorithms were employed to solve the Eqs. (16-19). Thus, in the present work, the SIMPLE algorithm was adopted to treat the pressure-velocity coupling, PRESTO! scheme for the pressure interpolation, *Least Squares Cell-Based* for the gradient discretization and *Second Order Upwind* for the advective terms of momentum and energy equations. As convergence criteria of the conservative equations, a residual of 10^{-6} was chosen for the mass and momentum, while a residual of 10^{-8} was admitted for the energy.

2.3.1 Mesh Quality Analysis

For the spatial discretization of the computational domain, structured grid meshes, consisting of quadrilateral cells, were used. A mesh refinement was applied in the regions near the cavity and IB walls, where the largest velocity and temperature gradients are observed. The mesh quality analysis was previously performed in Borahel et al. (2022a) through the GCI (*Grid Convergence Index*) method, proposed by Celik et al. (2008). At the time, three grid meshes were generated

and tested in the computational domain, each with a different number of cells. The uncertainty between them was determined considering three control parameters: v^*_{min} and v^*_{max} along the cavity horizontal mid-plane ($H^* = 0.5$) and q^*. The results obtained, which can be consulted in Borahel et al. (2022a), demonstrated that the most refined grid mesh (with 66.300 cells, shown in Fig. 3) – tested for the computational domain with $AR = 0.5$ and $AR_0 = 1$ – is indicated for the spatial discretization of the problem, so that all the other meshes were built from its parameters.

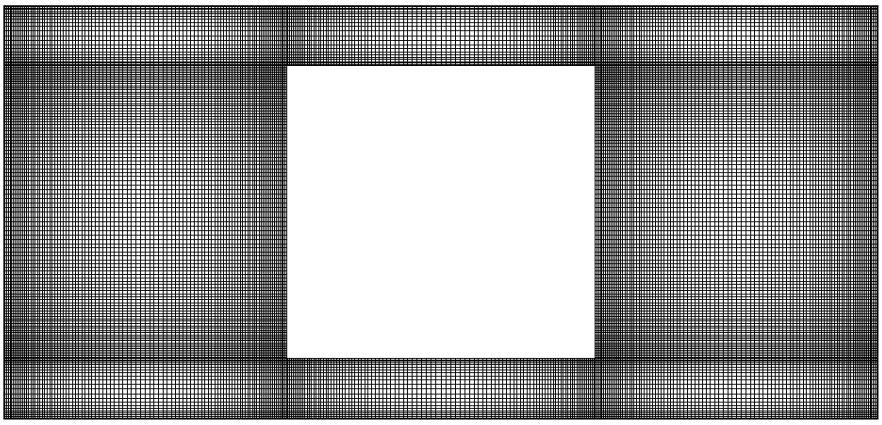

Figure 3. Most refined mesh used in the spatial discretization of the computational domain with $AR = 0.5$ and $AR_0 = 1$.

2.3.2 Model Verification

The model verification, necessary to ensure that the mathematical and numerical models are suitable for the proposed study, was previously conducted in Borahel et al. (2022a) and Borahel et al. (2022b), where further details regarding it can be found. Briefly, the validation procedures consisted of using the models implemented here to reproduce the numerical studies of Islam et al. (2012) and Moraga et al. (2017), where a square IB is cooled inside a lid-driven cavity for Ri = 0.1, 1.0 and 10. The results obtained showed that the implemented models were able to satisfactorily reproduce the u^* and v^* profiles obtained for Islam et al. (2012) and Moraga et al. (2017). Regarding the Nusselt number ($\underline{Nu}_{\sqrt{A}}$) on the IB walls, the highest percentage difference observed between the results obtained here and those presented by Islam et al. (2012) was only 1.78%, related to the dominant mixed convection (Ri = 1.0) cases. Therefore, it can be confidently stated that the models utilized are well-suited for the intended study.

3. RESULTS AND DISCUSSIONS

The effects of AR_0 and ψ on the dimensionless heat rate (q^*) inside the cavity are shown in Fig. 4 for each AR analyzed.

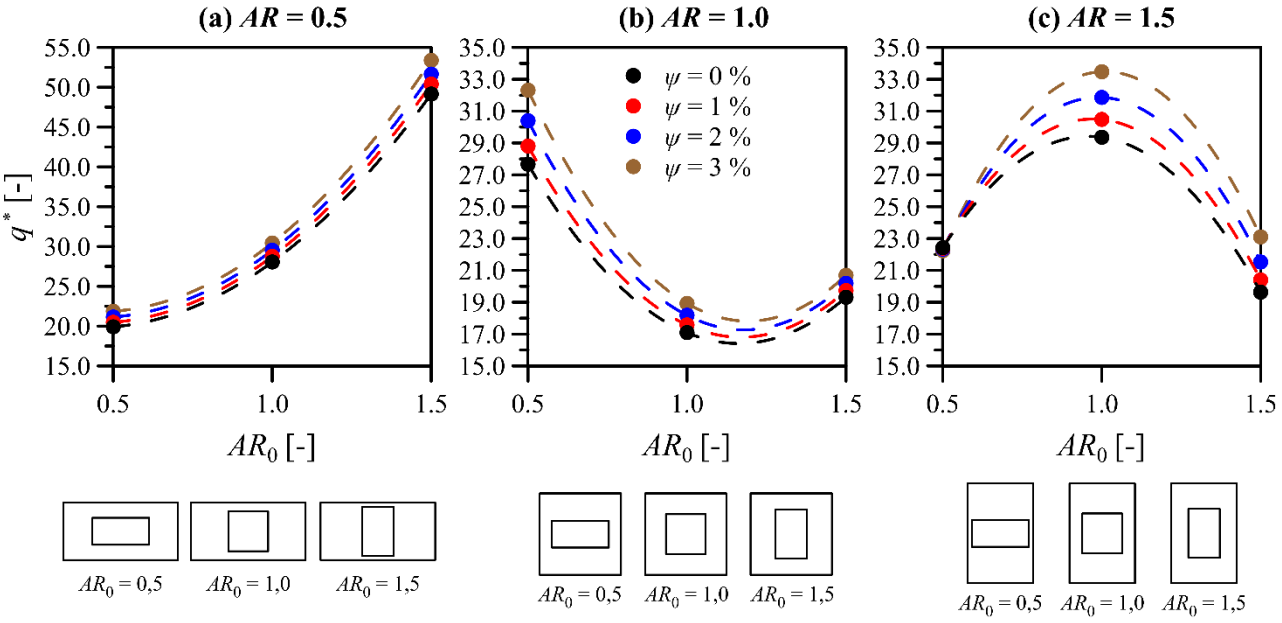

Figure 4. Effects of the IB area fraction (AR_0) on the dimensionless heat transfer rate (q^*) for (a) AR = 0.5, (b) AR = 1.0 and (c) AR = 1.5.

As can be seen in Fig. 4 (a), where the cavity has a horizontal shape (AR = 0.5), the convective heat transfer inside the cavity – denoted by q^* – increases as the IB aspect ratio (AR_0) and the nanofluid concentration (ψ) increase. On other words, q^* demonstrates an ascending behavior concerning AR_0 e ψ for the horizontal cavity. In Fig. 4 (b), for AR = 1.0 (square cavity), two distinct behaviors are observed for q^* depending on AR_0: descending between AR_0 = 0.5 and 1.0, and ascending between AR_0 = 1.0 and 1.5. Therefore, a minimum q^* is associated with AR_0 = 1.0, which is consistent with the previous findings published in Borahel et al. (2022b) for a square cavity with a BI of similar size to the one analyzed here. However, when considering the same IB aspect ratio (1.0) but with a tall-shaped cavity (AR = 1.5), the minimum q^* peak observed in Fig. 4 (b) transforms into a maximum peak, as depicted in Fig. 5 (b). This observation highlights the simultaneous influence of the block and cavity aspect ratios on the convective heat transfer. It indicates that for each specific cavity shape, there exists an optimal block shape, and vice versa. Among all the designs tested for the system, the best configuration was achieved by combining the lowest cavity aspect ratio (AR = 0.5) with the highest IB aspect ratio (AR_0 = 1.5). The increase in q^* for this design can be attributed to the horizontal shape of the cavity. This shape results in a larger lid wall, which increases the flow momentum and, consequently, intensifies the convective heat transfer. Additionally, the vertically elongated IB exhibits a larger perimeter, resulting in an increased heat exchange area, which also contributes to enhance the heat transfer.

Table 2 presents the impact of the nanofluid concentration (ψ) on the dimensionless heat transfer rate (q^*) for the various designs investigated for the system.

Table 2. Effects of the Al_2O_3 particles concentration (ψ) on the dimensionless heat transfer rate (q^*).

		Dimensionless Heat Transfer Rate (q^*)			
	AR_0	ψ = 0%	ψ = 1%	ψ = 2%	ψ = 3%
***AR* 0.5**	0.5	19.91	20.48	21.14	21.86
	1.0	28.04	28.75	29.52	30.44
	1.5	49.15	50.38	51.64	53.38
***AR* 1.0**	0.5	27.66	28.81	30.40	32.31
	1.0	17.09	17.57	18.18	18.92
	1.5	19.31	19.73	20.18	20.69
***AR* 1.5**	0.5	22,42	22,39	22,33	22,23
	1.0	29,36	30,47	31,86	33,47
	1.5	19,62	20,39	21,52	23,10

As can be seen in Tab. 2, for all the designs tested, except one (AR = 1.5; AR_0 = 0.5), the convective heat transfer inside the cavity was higher in the cases where the highest concentration of nanofluid was employed. For the best design (AR = 0.5; AR_0 = 1.5), q^* was increased from 49.15 to 53.38 by using the higher concentration nanofluid (ψ = 3%) instead of pure water (ψ = 0%). In percentage numbers, the dimensionless rate of heat transfer recorded for this design increased by approximately 8.6% through the mere insertion of Al_2O_3 nanoparticles into the base fluid. The highest percentage increase in the heat transfer, with respect to ψ, was observed for the configuration with AR and AR_0 equal to 1.5, where q^* was intensified by approximately 17.7% due to the use of the nanofluid with a concentration of particles equal to 3%. This improvement in the dimensionless heat transfer rate with the increase in the nanofluid concentration is attributed to its thermophysical properties, mainly its thermal conductivity. In summary, metallic nanoparticles have a large surface area compared to their volume. Additionally, the thermal conductivity of Al_2O_3 is more than 60 times higher than that of water (as shown in Table 1). As a result, any addition of metallic nanoparticles to the working fluid, even in small quantities as done in this study, leads to a significant increase in the fluid's thermal conductivity. For reference, the thermal conductivity of the more concentrated nanofluid (ψ = 3%) is approximately 10.6% higher than that of the base fluid, which directly affects the heat transfer and justifies the superior thermal performance observed for the cases where the highest nanoparticle concentration was admitted.

A more comprehensive understanding of how the thermal and fluid dynamic characteristics of the flow are influenced by the geometric parameters of system (AR and AR_0 = 0.5) and nanofluid concentration (ψ) can be obtained in Fig. 5, where the dimensionless temperature (θ^*) fields and velocity vectors inside the cavity are presented for two different system design: (i) AR = 0.5; AR_0 = 1.5 and (ii) AR = 1.5; AR_0 = 0.5.

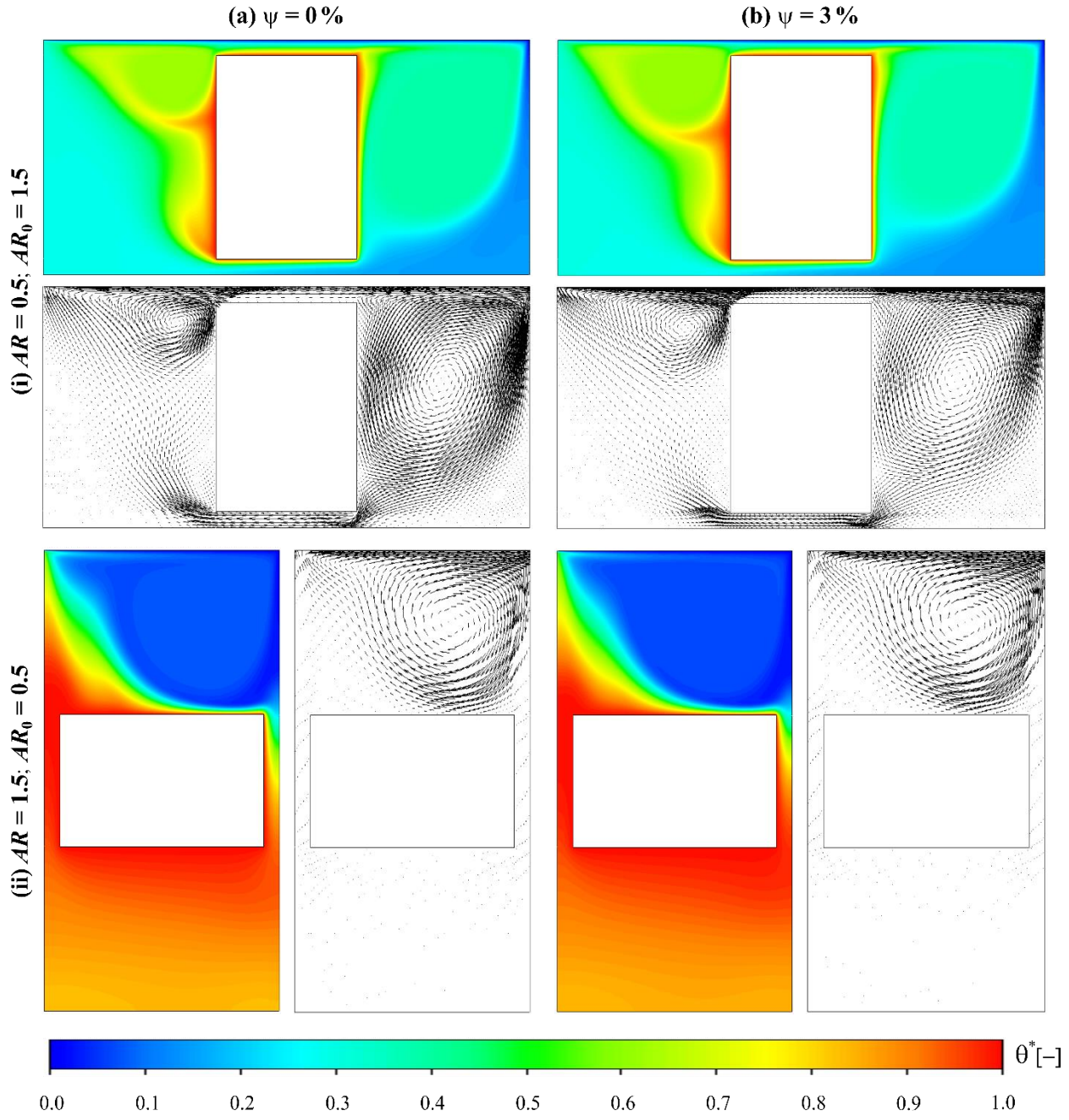

Figure 5. θ^* fields and velocity vectors inside the cavity for two different system design: (i) AR = 0.5; AR_0 = 1.5 and (ii) AR = 1.5; AR_0 = 0.5; where (a) ψ = 0 % and (b) ψ = 3 %.

As can be seen in Fig. 5, the temperature fields and flow dynamics remain unchanged with the addition of nanoparticles into the fluid. Hence, it becomes evident that the q^* increments observed in Table 2 – when ψ is increased – are solely attributed to the alterations that arise in the fluid's properties as a direct result of the nanoparticle incorporation. Regardless of ψ, the flow behavior and the temperature fields associated with it have been shown to be dependent on the geometric configuration of the system. For the horizontal cavity (AR = 0.5), with the IB exhibiting a tall shape (AR_0 = 1.5), the convective flow encompasses the entire system, as illustrated in Fig. 5 [(a-b) (i)]. In the upper and lower channels of the system, which correspond to the regions between the IB and the upper and lower cavity walls, a horizontal unidirectional flow is observed, resembling the patterns commonly found inside ducts or pipelines. Clockwise convective cells are noted in both lateral channels of the system. On the left, a small convective cell can be seen, whose action is restricted to the upper region of the channel, close to the IB. On the other hand, almost the entire right channel of the system is occupied by the convective cell that forms there, which accelerates the flow and, consequently, contributes to the heat transfer, as explained by Borahel et al. (2022a). In other words, the flow dynamics associated with this design are favorable for the heat transfer. The combined effect of this factor, along with those previously discussed (larger IB thermal exchange area and greater momentum induced by the lid wall on the flow due to its elongated dimension),

elucidates why this specific design proven to be the most suitable for promoting the heat transfer within the cavity. In the opposite design [Fig. 5 (a-b) (ii)], characterized by a tall cavity shape ($AR = 1.5$) with a IB horizontally elongated ($AR_0 = 0.5$), a flow pattern detrimental to the convective heat transfer is observed. In this design, the high horizontal occupancy of the cavity leads to reduced dimensions of the lateral channels of the system, which hinder the free circulation of the flow. As a result, the flow within the cavity is restricted to the upper channel, so that the convective heat transfer on the bottom and lateral walls of the isothermal block is practically nil.

4. CONCLUSIONS

Employing the constructal design method, associated with an exhaustive search approach, the aim of this numerical work was to evaluate and maximize the convective heat transfer between an isothermal block (IB) and the surrounding flow in a lid-driven cavity. As working fluid, a metallic nanofluid consisting of a mixture of water and Al_2O_3 nanoparticles was adopted. The effects of the particle concentration (ψ) on the flow and convective heat transfer were evaluated for four different concentrations: 0%, 1%, 2% and 3%. For the system, the degrees of freedom (DOF) admitted were the aspect ratios of the isothermal block and cavity, while their areas were assumed as constraints. A total of 36 unique configurations were examined for the problem, resulting in an equal number of numerical simulations carried out in the commercial software ANSYS Fluent 2022 R2. Based on the results obtained, the following conclusions/findings can be drawn:

i) For the square cavity ($AR = 1.0$), the convective heat transfer, characterized by the dimensionless heat transfer rate (q^*), was found to be negatively affected by the isothermal block aspect ratio (AR_0) equal to 1. However, intriguingly, this block aspect ratio propitiated the highest values of q^* when a tall shape ($AR = 1.5$) was tested for the cavity. This behavior emphasizes the simultaneous influence of the block and cavity aspect ratios on the convective heat transfer, indicating that for each specific cavity shape, there exists an optimal isothermal block shape.

ii) In almost all designs tested for the system, the convective heat transfer was enhanced with increasing nanofluid concentration (ψ). For the geometric configuration with both the cavity and the isothermal block presenting a tall shape (AR and AR_0 equal to 1.5), q^* increased by approximately 17.7% when the most concentrated nanofluid ($\psi = 3\%$) was used instead of pure water ($\psi = 0\%$). This behavior can be attributed to the thermophysical properties of the nanofluid, specifically its thermal conductivity, which increases due to the nanoparticle incorporation in the base fluid.

iii) The best geometric configuration for the system was achieved by combining the lowest cavity aspect ratio ($AR = 0.5$) with the highest isothermal block aspect ratio ($AR_0 = 1.5$). This design features a larger lid wall, leading to increased flow momentum, as well as a larger thermal exchange area of the isothermal block, which enhances its heat transfer. The combined effect of these two factors, along with the favorable flow pattern observed for this design, explains why the maximum q^* obtained (53.38) is associated with this configuration.

5. ACKNOWLEDGEMENTS

The authors acknowledge the agencies CAPES, CNPq, FAPERGS (Proc. No. 21/2551-0002169-1) and the UNISINOS Academic Research and Postgraduate Unit. R.S. Borahel and P.M. Rodrigues have a doctorate degree scholarship financed by CAPES (Code 001). F.S.F. Zinani is a grant holder of CNPq (Proc. No. 311444/2021-0). L.A.O. Rocha is a grant holder of CNPq (Proc. No. 307791/2019-0).

6. REFERENCES

Alsabery, A.I., Armaghani, T., Chamkha, A.J. and Hashim, I., 2020. Two-phase nanofluid model and magnetic field effects on mixed convection in a lid-driven cavity containing heated triangular wall, Alexandria Engineering Journal, Vol. 59, n. 1, p. 129–148.

Bejan, A. and Lorente, S., 2008. *Design with constructal theory*. Editora John Wiley & Sons Inc, New Jersey.

Borahel, R.S., Zinani, F.S.F. and Rocha, L.A.O., 2022a. "Cooling by mixed convection of a heated obstacle in a lid-driven cavity of different aspect ratios: a constructal design study". In *Proceedings of the 19th Brazilian Congress of Thermal Sciences and Engineering - ENCIT 2022*. Bento Gonçalves, Brazil.

Borahel, R.S., Zinani, F.S.F., Rocha, L.A.O. and Biserni, C., 2022b. Geometric optimization of a rectangular isothermal block inside a lid-driven cavity by means of constructal design, International Communications of Heat and Mass Transfer, Vol. 139, p. 106499.

Celik, I.B., Ghia, U., Roache, P.J., Freitas, C.J., Coleman, H. and Raad, P.E., 2008. Procedure for estimation and reporting of uncertainty due to discretization in CFD applications, Journal of Fluids Engineering, Vol. 130.

Cunegatto, E.H.T., Gotardo, M. and Zinani, F.S.F., 2023. Numerical analysis of tube arrangements with one, two, and four degrees of freedom for heat transfer with pseudoplastic fluids, International Journal of Heat and Mass Transfer, Vol. 208, p. 124080.

Gangawane, K.M., Oztop, H.F. and Abu-Hamdeh, N., 2018. Mixed convection characteristic in a lid-driven cavity containing heated triangular block: Effect of location and size of block, International Journal of Heat and Mass Transfer, Vol. 124, p. 860–875.

Herouz, K., Laidoudi, H., Aissa, A., Mourad, A., Guedri, K., Oreijah, M. and Younis, O., 2023. Analysis of nano-encapsulated phase change material confined in a double lid-driven hexagonal porous chamber with an obstacle under magnetic field, Journal of Energy Storage, Vol. 61, p. 106736.

Islam, A.W., Sharif, M.A.R. and Carlson, E.S., 2012. Mixed convection in a lid driven square cavity with an isothermally heated square blockage inside, International Journal of Heat and Mass Transfer, Vol. 55, p. 5244-5255.

Kareem, A.K. and Gao, S.A., 2018. Comparison study of mixed convection heat transfer of turbulent nanofluid flow in a three-dimensional lid-driven enclosure with a clockwise versus an anticlockwise rotating cylinder, International Communications in Heat and Mass Transfer, Vol. 90, p. 44–55.

Kumar, S., Gangawane, K.M. and Oztop, H.F.A., 2021. Numerical study of mixed convection in a two-sided lid-driven tall cavity containing a heated triangular block for non-Newtonian power-law fluids, Heat Transfer, Vol. 50, n. 5, p. 4806–4829.

Moraga, N.O., Marambio, M.A. and Cabrales, R.C., 2017. Geometric multigrid technique for solving heat convection-diffusion and phase change problems, International Communications of Heat and Mass Transfer, Vol. 88, p. 108-119.

Prasad, A.K. and Koseff, J.R., 1996. Combined forced and natural convection heat transfer in a deep lid-driven cavity flow, International Journal of Heat and Fluid Flow, Vol. 17, n. 5. p. 460-467.

Rais, A.I., Mahmud, M.J., Hossain, M.R. and Saha, S., 2023. Influence of heat generation/absorption on mixed convective flow in a lid-driven chamber with isothermal rotating cylinder, Annals of Nuclear Energy, Vol. 182, p. 109596.

Razera, A.L., da Fonseca, R.J.C., Isoldi, L.A., dos Santos, E.D., Rocha, L.A.O. and Biserni, C., 2022. A constructal approach applied to the cooling of semi-elliptical blocks assembled into a rectangular channel under forced convection, International Journal of Heat and Mass Transfer, Vol. 184, p. 122293.

Razera, A.L., da Fonseca, R.J.C., Isoldi, L.A., dos Santos, E.D., Rocha, L.A.O. and Biserni, C., 2018. Constructal design of a semi-elliptical fin inserted in a lid-driven square cavity with mixed convection, International Journal of Heat and Mass Transfer, Vol. 126, p. 81–94.

Rodrigues, P.M., Biserni, C., de Escobar, C.C., Rocha, L.A.O., Isoldi, L.A. and dos Santos, E.D., 2020. Geometric optimization of a lid-driven cavity with two rectangular intrusions under mixed convection heat transfer: A numerical investigation motivated by constructal design, International Communications of Heat and Mass Transfer, Vol. 117. p. 104759

Shulepova, E.M., Sheremet, M.A., Oztop, H.F. and Abu-Hamdeh, N., 2020. Mixed convection of Al_2O_3-H_2O nanofluid in a square chamber with complicated fin, International Journal of Mechanical Sciences, Vol. 165, p. 105192.

Younis, O., Ahmed, S.E., Abderrahmane, A., Alenazi, A. and Hassan, A.M., 2023. Hydrothermal Mixed Convection in a Split-Lid-Driven Triangular Cavity Suspended by NEPCM, Mathematics, Vol. 11, n. 6, p. 1323.

7. RESPONSIBILITY NOTICE

The authors are the only responsible for the printed material included in this paper.